Monte Carlo model for multiparticle production at ultrarelativistic energies

N. S. Amelin,* H. Stöcker, and W. Greiner
Institut für Theoretische Physik, Universität Frankfurt, Postfach 111932, D-6054 Frankfurt am Main 11, Germany

N. Armesto, M. A. Braun,† and C. Pajares
Departamento de Física de Partículas, Universidade de Santiago de Compostela, 15706-Santiago de Compostela, Spain
(Received 22 February 1994; revised manuscript received 19 December 1994)

The Monte Carlo parton string model for multiparticle production in hadron-hadron, hadron-nucleus, and nucleus-nucleus collisions at high energies is described. An adequate choice of the parameters in the model gives the possibility of recovering the main results of the dual parton model, with the advantage of treating both hadron and nuclear interactions on the same footing, reducing them to interactions between partons. Also the possibility of considering both soft and hard parton interactions is introduced. Comparison to the available experimental data on nucleon and nuclear collisions, together with predictions for mean multiplicities, net baryon rapidity distributions, and the temporal evolution of meson densities for heavy ion collisions at the CERN Super Proton Synchrotron (194A GeV) and the BNL Relativistic Heavy Ion Collider (200A GeV) are presented. Furthermore, predictions for charm production at these energies are given.

I. INTRODUCTION

The search for the quark-gluon plasma (QGP) is the goal of the experimental heavy-ion program [1]. Nevertheless, no conclusive evidence of the existence of such a deconfined state of matter arises from the data coming from Brookhaven [Alternating Gradient Synchrotron (AGS)] and CERN [Super Proton Synchrotron (SPS)]. Models containing no QGP formation, like those based on the production of color strings which decay independently into the observed hadrons, are able to describe the bulk of the data [2–6]. Up to now the data are limited to relatively light projectiles and energies in the range $E_{\rm lab} = (10\text{–}200)A$ GeV. Massive ion beams, whose collisions are expected to lead to the creation of extremely dense hadronic matter, will be available up to collider energies $E_{\rm c.m.} = 100A$ GeV at Brookhaven [Relativistic Heavy Ion Collider (RHIC)] and $E_{\rm c.m.} = 3000A$ GeV at CERN [Large Hadron Collider (LHC)]. With increasing energy a change in the hadron production mechanism is expected. At lower energies hadrons are produced essentially in soft collisions with small transferred momenta; at collider energies the so-called semihard processes [which can be calculated using perturbative quantum chromodynamics (PQCD) [7]] will dominate.

The string models quoted above are essentially hadron-based models. In these models the nuclear interactions are reduced to hadron interactions. Quark and gluon degrees of freedom are used only to compute particle production at the hadronic stage. In hadron cascade models [3,6] the interaction with the nuclear target is realized by successive interactions with separate nucleons. Other models treat nuclear interactions as "simultaneous" interactions with different nucleons in the target [2,4,5]. For both approaches to be valid the density of the hadronic matter has to be low to be able to distinguish between interactions with two different nucleons. Also, in this manner one can study the evolution of the colliding system only at a size scale larger than the hadronic one.

In view of the high hadronic density which is going to be achieved in heavy-ion collisions in new experiments, this hadron-based approach seems unsatisfactory. The correct way to study nuclear collisions at high hadronic density is evidently to employ the parton picture from the start and so to treat the nucleus as a "big hadron," on equal footing with the nucleon. The present model for nucleus collisions is set up to achieve this goal: the so-called loop diagrams and groups of overlapping nucleons which appear in the full Glauber model (see, for example, Ref. [8]) and grow in importance with increasing hadronic densities are naturally taken into account in our approach, while in the models quoted above they are neglected or considered only in some crude approximations. Nevertheless, as discussed in Ref. [8], the observable influence of these configurations is subtle, inducing, for example, no change in the multiplicity. Some effect could be seen on observables sensitive to the nuclear edge, such as nuclear diffraction (for a discussion on the influence of the breakdown of the factorization hypothesis in Glauber and string fusion on diffraction in hadron-nucleus collisions see Ref. [9]).

The main novel feature of our model is the way we describe the colliding nuclei. We treat them in the same way as hadrons are treated in current models: the nucleus is considered to be a superposition of partons (quarks, antiquarks, diquarks, and gluons) with a variable number

*On leave of absence from the JINR, Dubna, Russia.
†On leave of absence from the Department of High Energy Physics, University of St. Petersburg, 198904 St. Petersburg, Russia.

and a distribution which is a convolution of the parton distribution in the nucleon and the nucleon distribution in the nucleus. The nuclear collision is then a superposition of partonic collisions. Particle production in these latter is described by color string formation and decay, more or less in the same manner as in the dual parton model (DPM) [10].

The analytical quark-gluon string model (QGSM) [11] reproduces satisfactorily the cross sections and spectra of charmed particles produced in nucleon and nuclear collisions (see Refs. [12,13]). A more common approach is to consider heavy flavor production in the framework of the PQCD (see, for example, Ref. [14]). However, this approach also requires a nonperturbative input for the hadronic and nuclear structure functions. The color string picture combines the nonperturbative and perturbative aspects of the heavy flavor production into the formation of strings and their decay into high mass states. It may then be considered as a dynamical alternative to the PQCD plus given structure functions. Predictions of the QGSM and PQCD (with absorptive corrections) are shown to coincide through a large energy range [13], although there are some differences already in hh collisions: for example, the x_F spectrum of Λ_c's in pp collisions at $\sqrt{s} = 62$ GeV is correctly described by the QGSM, while PQCD (without additional mechanisms like intrinsic charm) shows a behavior opposite to the experimental data [15]. In our model the QGSM-like description of heavy flavor production allows us to obtain a unified picture of production of particles of all flavors with a minimal number of assumptions (and parameters); in addition, the extension of charm calculations to the case of hA and AB collisions is made just in the same way as for light flavor production, i.e., without new assumptions, while in PQCD some hypothesis about the nuclear shadowing of the structure functions (whose influence arises mainly at large x_F) is needed.

This paper is organized as follows. In the next section, the Monte Carlo parton string model in described (a first description of this numerical model can be found in Ref. [16], where the influence of string interaction on multiple production was studied). In Sec. III, comparison to experimental data for hadron and nucleus collisions at SPS and S$p\bar{p}$S energies is presented, together with a comparison to charm data in pp collisions at $E_{\text{c.m.}} = 27$ GeV. In Sec. IV we distinguish between soft and hard parton interactions, as required by the data: In addition to soft parton collisions, in which the transferred momenta are neglected, hard perturbative parton-parton collisions and parton bremsstrahlung are introduced. In Sec. V predictions for mean multiplicities of light and charmed hadrons, for the nuclear stopping power, and for the evolution of the colliding system in heavy-ion collisions are presented. Finally in Sec. VI our conclusions are given.

II. MODEL DESCRIPTION

The main components of our model are as follows.

(i) The main new feature of the model, as stated in the Introduction, is the way we describe nuclear collisions. For these we construct the nuclear parton wave function as a convolution of parton distributions of individual nucleons with the distribution of nucleons inside the nucleus. The position of each nucleon is taken to be described by the Woods-Saxon density

$$\rho(r) = \rho_0/\{1 + \exp[(r - r_0)/a]\}, \tag{1}$$

with

$$r_0 = 1.19A^{1/3} + 1.61A^{-1/3} \text{ fm}, \quad a = 0.54 \text{ fm}. \tag{2}$$

To take the Fermi motion of nucleons into account we generate a Fermi momentum p for each nucleon uniformly distributed in the range $0 < p < p_F$, where p_F is the maximum Fermi nucleon momentum,

$$p_F = (3\pi^2)^{1/3} h \rho^{1/3}(r), \tag{3}$$

with $h = 0.197$ fm GeV/c. An isotropical angular distribution is assumed in both the coordinate and momentum spaces.

(ii) As to the parton distribution for individual nucleons, this is taken to be the same as for NN collisions. In particular, the distribution in the number of partons of a given flavor F in a nucleon, which is directly connected with the value of the multi-Pomeron vertices in the Reggeon theory [17], is taken to be Poissonian:

$$w_N = C_F \exp[-g(s)] g^N(s)/N!, \tag{4}$$

corresponding to the eikonal picture, $\sum C_F = 1$. The mean number of partons in each nucleon, $g(s) = g_0 s^{\Delta}$, is a function of the center of mass energy $\sqrt{s}$. We use $g_0 = 3.0$ and $\Delta = 0.09$. The ratio of sea strange quarks to sea up and down quarks is 0.3:1:1 as in string fragmentation. No sea charmed quarks have been introduced.

The parton distribution in impact parameter (relative to the center of the corresponding nucleon) is taken to be Gaussian, in accordance with the Pomeron picture of strong interactions:

$$F(b_p) = (4\pi\lambda)^{-1} \exp(-b_p^2/4\lambda), \tag{5}$$

with the radius depending on the initial nucleon energy. For a projectile or target nucleon, $\lambda = R^2 + \alpha' \ln\sqrt{s}$, where $\alpha' = 0.01$ fm^2 and $R^2 = 0.15$ fm^2. So a Gaussian form is also taken for the p_t distribution of partons:

$$f(p_t^2) p_t dp_t \sim \exp(-b p_t^2) p_t dp_t, \tag{6}$$

with $b = 4$ GeV^{-2}.

The nucleon structure function in $x_{\pm} = p_{\pm}/P_{\pm}$ ($p_{\pm}$ the momenta of the partons and $P_{\pm}$ the momentum of the nucleon they belong to) is assumed factorized, except for energy-momentum conservation:

$$u(x_1, x_2, \ldots, x_N) = \delta\left(1 - \sum_{i=1}^{N} x_i\right) \prod_{i=1}^{N} u_i(x_i). \tag{7}$$

For the single parton distributions $u_i(x)$, the ones obtained from the Regge theory are used [11]:

$$u_v(x) = u_s(x) \propto x^{-0.5}, \quad u_{vv}(x) \propto x^{1.5}, \tag{8}$$

except for gluons and strange sea quarks, for which $u_s(x) \propto 1/x$ is used. v, s, and vv refer to valence and sea quarks and diquarks, respectively. In all cases, a cutoff in x ($x > x_{\min} = m_t/P_+$, m_t being the transverse mass of the parton) is employed. This will ensure that the strings have mass enough to be projected onto a hadron with the adequate flavor content.

(iii) A hadron or nucleus collision is assumed to be the interaction between partons from the projectile and target. A parton from the projectile can interact with one from the target if they lie in impact parameter space within an area determined by the parton-parton cross section, which has been assumed energy independent, $\sigma_p = 3.5$ mb. In this way the number of inelastic collisions is determined and the inelastic cross section is calculated (an elastic event is one with no partons close enough in impact parameter space).

As in the standard dual parton model [10,11], we assume that each parton interaction creates a color string which subsequently decays into hadrons. Since both the projectile and target nucleon should remain colorless, color strings should be created in pairs. Each pair of color strings corresponds to the cut Pomeron of the Reggeon theory. Only quarks (and diquarks) are assumed to produce strings. Gluons are effectively taken into account as $q\bar{q}$ pairs (in the spirit of the large N_c expansion of QCD, which lies at the basis of the DPM). Neither multiple interactions of the same parton nor diagrams with an odd number of strings are taken into account (these contributions die out at high energies).

The quality of the choice of the parton distributions and the cross section σ_p is demonstrated in Fig. 1, where the inelastic NN cross sections are compared to experimental data. Figure 2 shows the dependence of the average number of parton collisions $\langle N^p_{\rm coll}\rangle$ on the impact parameter b, in pp interactions at SPS, RHIC, and LHC energies. In central collisions (here and further on, a central collision means $b = 0$), this value changes from 2 at 19.4 GeV to 8 at 6300 GeV. The distribution in the number of interacting nucleons from the projectile nucleus is

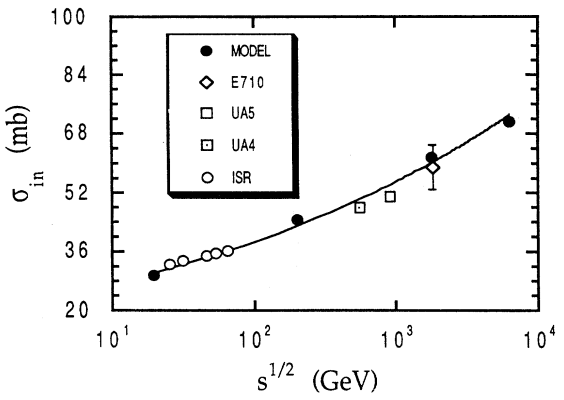

FIG. 1. Nucleon inelastic cross sections as a function of energy. Black circles are the result of the calculation, open symbols are the experimental data.

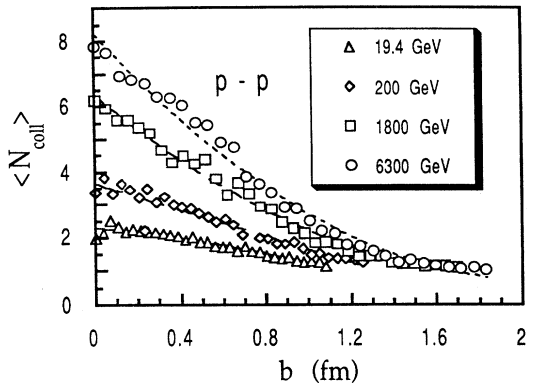

FIG. 2. Predictions of the model for the mean number of parton-parton collisions as a function of the impact parameter, in pp interactions, at (from the bottom to the top) $E_{\rm c.m.} = 19.4$, 200, 1800, and 6300 GeV.

presented in Fig. 3, for O-Au collisions at 200A GeV, in comparison with the predictions of the VENUS model [4] (which correspond to the Glauber model). They look quite similar. The distribution in the number of interacting partons is also shown in this figure.

(iv) The produced strings decay into hadrons. The approaches most commonly used to describe the string decay are the Artru-Mennessier model [18], the Field-Feynman algorithm [19], and the most popular one, the Lund fragmentation model [20,21]. All of them treat the

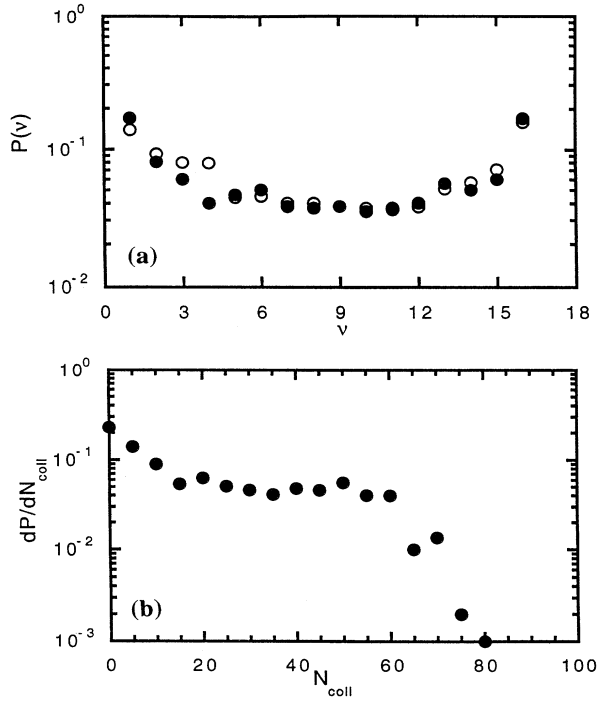

FIG. 3. (a) Calculated distribution (open circles) of the number of participating projectile nucleons, compared to the VENUS model [4] predictions (black circles). (b) Distribution in the number of parton-parton collisions. Both figures are for OAu collisions at 200A GeV.

string decay through the creation of quark-antiquark or diquark-antidiquark pairs with transverse masses. In all models, the parameters are extracted from the comparison to e^+e^- and lN data. In this sense, they give equal results for hadron collisions.

In our case, the modeling of the decay of a string with a given mass, momentum, and quark content is carried out by the Field-Feynman algorithm [19]. The flavor content at each string breakup is determined using a strangeness suppression parameter $\gamma_{s\bar{s}} = 0.3$ and a ratio of diquark-antidiquark pair production to quark-antiquark one equal to $P_{qq,\bar{q}\bar{q}}:P_{q\bar{q}} = \gamma_{B\bar{B}} = 0.09$. Charmed quarks appear at this stage. The spin of the produced particles is introduced in the usual way [20,21]. At a string breakup the $q\bar{q}$ pair has zero total transverse momentum, the momenta of the quark $\mathbf{p}_t$ and the corresponding antiquark $-\mathbf{p}_t$ being distributed according to Eq. (6), with $b = 8.2$ $(\mathrm{GeV}/c)^{-2}$. The transverse momentum of a produced hadron is the sum of the transverse momenta of its quarks, and its longitudinal momentum p_z^h and energy E^h are determined through the variable $z = (E^h + p_z^h)/(E^q + p_z^q)$ (E^q being the energy and p_z^q the longitudinal momentum of the fragmenting quark), with the following distribution:

$$f_h^g(z) \sim (1-z)^{\alpha_q^h(p_t)}. \tag{9}$$

At $z \to 1$, this function coincides with the fragmentation function $D_q^h(z)$ of the leading quark (antiquark) or diquark (antidiquark) into a hadron. $\alpha_q^h(p_t)$ depends on the flavor of the constituent quark and on the type of hadron it is transformed into and its momentum. It can be related to the Regge trajectory of the particle exchanged [11]. For example, if there is a $\bar{u}$ quark at the end of a string and a D^0 is produced at this end, a $c\bar{c}$ pair has to be created, so that the exponent $\alpha_q^h(p_t)$ is related to the Regge trajectory of the ψ family; in this way we obtain a D^0 and a shorter string with a $\bar{c}$ quark at the corresponding end.

The requirement that the fragmentation function $D_q^h(z) \to 1/z$, for $z \to 0$, is ensured by iterating string breakups. If the mass of a string, M_s, is less than $M_c = M_R + \Delta M$, where $\Delta M = 0.35$ GeV and M_R is the mass of the resonance with the same quark composition as the string, the last break is generated. Its kinematics is determined by the isotropy of the emission of two hadrons. The newly produced resonances are assumed unpolarized, and hence they decay isotropically, for which the experimentally known branching ratios are used.

III. COMPARISON TO EXPERIMENTAL DATA

A. The data at $E_{\mathrm{c.m.}} = 19.4A$ GeV

In Figs. 4 and 5, the results of the model for proton-proton, proton-nucleus, and nucleus-nucleus collisions at $E_{\mathrm{c.m.}} = 19.4A$ GeV (CERN SPS) are compared with experimental data. From Fig. 4 we conclude that the model reproduces successfully the experimental rapidity and multiplicity distributions for negative particles. It also describes satisfactorily the strange hadron production in pp and pA collisions [16], except the shape of the rapidity distribution of Λ's measured by the NA35 Collaboration [23]. However, the model does not predict any low p_t enhancement, which is visible in the NA35 experiment for central SS collisions, and more pronounced for heavier colliding systems [24]. As was demonstrated earlier [16], our model (without additional mechanisms) fails to reproduce the mean number of strange baryons and their rapidity distributions in central SS collisions.

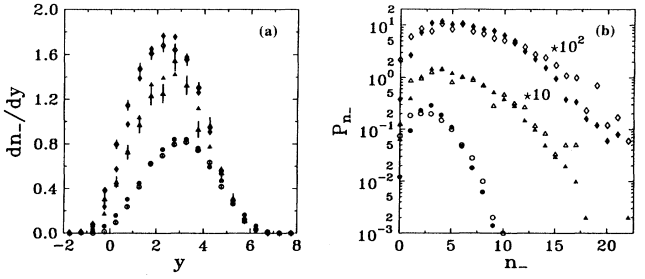

FIG. 4. (a) Rapidity and (b) multiplicity distributions of negative particles in pp (circles), pAr (triangles), and pXe (diamonds) collisions. The open points are experimental data [22]; the black ones are model predictions.

Proton transverse momentum distributions in nuclear collisions (shown in Fig. 5) are very sensitive to the chosen primordial quark momenta and can be fitted by changing some parameters. Since nuclear cascading of secondaries is not taken into account, our model is not able to reproduce positive particle (proton) rapidity distributions in the nucleus fragmentation region. It is known [3,6] that secondary cascading can improve the description of the proton rapidity distributions. It also changes essentially transverse momentum distributions, particularly the low momentum pion distribution, as a result of creation and decay of Δ resonances. In addition, it can enhance strangeness production on nuclear targets due to resonance-nucleon interactions.

B. Charm production

In our Monte Carlo approach the fragmentation functions shown in Eq. (9), taken from Ref. [11], are used.

TABLE I. Model prediction for charmed meson production in pp interactions at $E_{\mathrm{c.m.}} = 27.4$ GeV, compared to experimental data [25].

Meson	Expt. cross section (μb)	Mod. cross section (μb)	Mean multiplicity
D^+	5.7±1.0	10.35	0.000 35
D^-	6.2±1.0	12.48	0.000 41
D^0	10.5±1.7	10.35	0.000 34
$\bar{D}^0$	7.9±1.5	19.17	0.000 63

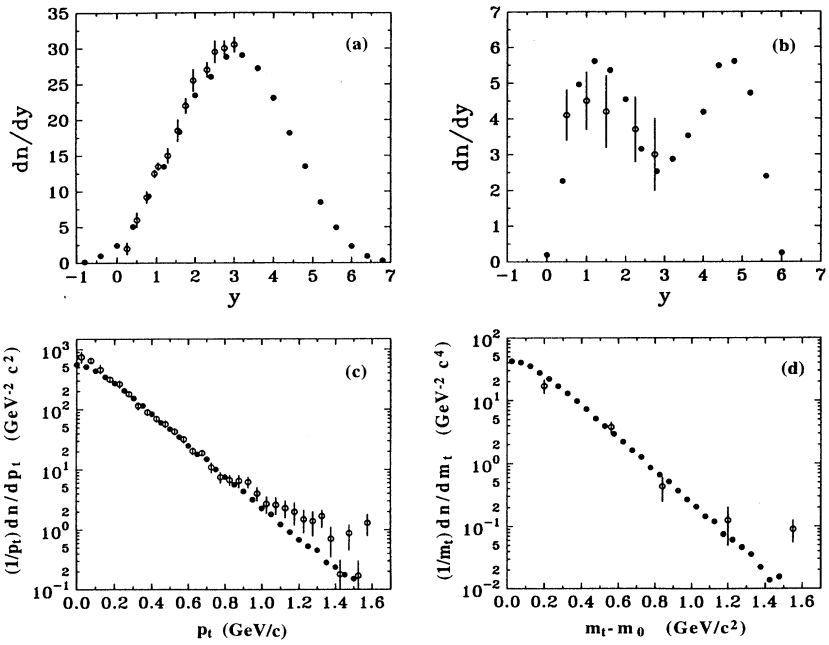

FIG. 5. Rapidity [(a),(b)] and transverse momentum [(c),(d)] distributions of negative particles [(a),(c)] and protons [(b),(d)] in central SS collisions. The transverse momentum distributions of negative particles and protons are in the rapidity interval $0.8 < y < 2.0$. The open points are data [23]; the black ones are model predictions.

The exponent $\alpha_q^h(p_t)$ is eventually determined [11] by the intercept of the Regge trajectory α_ψ for the ψ family, not well known. Our choice is $\alpha_\psi = -2.2$. A suppression parameter for production of charmed quark pairs (as for strange quark pairs) in string fragmentation is used: from comparison to the experimental data [25], $\gamma_{c\bar{c}} = 0.0025$. Cross sections for different charmed particles are compared with the experimental data in Table I, for 100 000 simulated events. This statistics is too small to extract x distributions for different particles, but enough to show the prediction of the model for all D mesons (Fig. 6).

C. The data at $E_{\text{c.m.}} = 200A$ GeV

In Table II we compare the mean numbers of particles produced to the experimental data for $\bar{p}p$ collisions at $E_{\text{c.m.}} = 200A$ GeV. The production of strange particles and antibaryons is fully determined by the fragmentation parameters: the strangeness and baryon-antibaryon suppression factors described in Sec. II. In Fig. 7, some experimental data are plotted together with the model predictions. With the exception of the low multiplicity event underestimation, the model reproduces well the experimental data. The reason for this discrepancy might be connected with the fragmentation procedure, or with the necessity of including some additional mechanism, like diffraction.

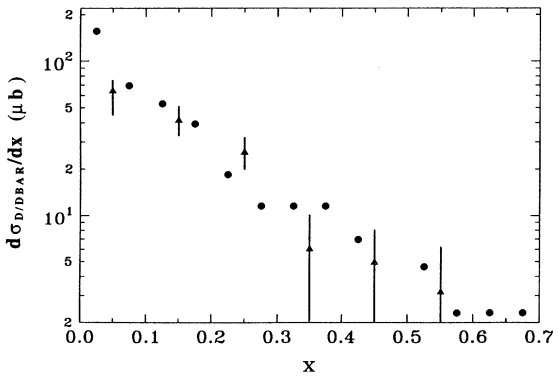

FIG. 6. Inclusive x spectrum of all D mesons produced in pp interactions at $E_{\text{c.m.}} = 27.4$ GeV. Black circles are model predictions; triangles with errors bars are data taken from Ref. [25].

IV. INCLUSION OF HARD PARTON SCATTERING

So far, only soft interactions between partons have been considered: no momentum, only color charge, can be transferred during each parton collision. The picture

TABLE II. Experimental data [26] and model predictions on the average number of given particles, in $p\bar{p}$ interactions at $E_{\text{c.m.}} = 200$ GeV.

Hadron multiplicity	Expt.	Model
$n_{\text{ch}}(-3.5 < \eta < 3.5)$	17.6± 0.2	16.95
$n_{K^0_s}(-3.5 < y < 3.5)$	0.71±0.08	0.78
$n_{K^\pm}(-3.5 < \eta < 3.5)$	1.15±0.13	1.50
$n_{n+\bar{n}}(-0.5 < y < 0.5)$	0.07±0.03	0.12
$n_{p+\bar{p}}(-3.5 < \eta < 3.5)$	0.6 ± 0.3	0.55
$n_{\Lambda+\bar{\Lambda}+\Sigma^0+\bar{\Sigma}^0}(-2.0 < y < 2.0)$	0.26±0.08	0.25
$n_{\Lambda+\bar{\Lambda}+\Sigma^0+\bar{\Sigma}^0}(-3.5 < \eta < 3.5)$	0.31±0.09	0.29
$n_{\Sigma^\pm+\bar{\Sigma}^\pm}(-3.5 < \eta < 3.5)$	0.16±0.06	0.096
$n_{\Xi^-+\bar{\Xi}^-}(-3.0 < y < 3.0)$	0.03±0.03	0.028
$n_{\Xi^-+\bar{\Xi}^-}(-3.5 < \eta < 3.5)$	0.03±0.03	0.024
$n_{\pi^\pm}(-3.5 < y < 3.5)$	15.9± 0.4	15.27

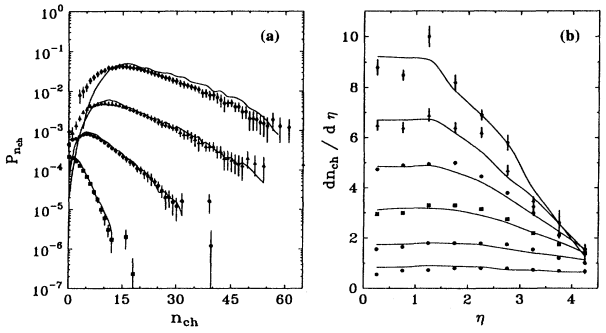

FIG. 7. (a) Multiplicity distributions for charged particles in different pseudorapidity intervals [from the bottom to the top, $|\eta| < 0.5$ ($\times 10^3$), $|\eta| < 1.5$ ($\times 10^{-2}$), $|\eta| < 3.0$ ($\times 10^{-1}$) and full phase space] and (b) semi-inclusive pseudorapidity distributions for different multiplicity bins ($2 \leq n \leq 10$, $12 \leq n \leq 20$, $22 \leq n \leq 30$, $32 \leq n \leq 40$, $42 \leq n \leq 50$, and $52 \leq n$) in nonsingle diffractive $p\bar{p}$ events at $E_{\text{c.m.}} = 200$ GeV, together with experimental data [27,28]. Full lines are model predictions; black symbols are experimental data.

of the interaction is an even number of longitudinal color strings, spanned between color triplet quarks or diquarks, moving into opposite directions in the string rest frame. In fact, quarks carry all energy-momentum and no gluons appear explicitly in the model. Anyway, gluons are implicit in the fragmentation mechanism [20] and are effectively present as sea quark-antiquark pairs, as explained in Sec. II.

At SPS energy the soft mechanism is enough to satisfactorily reproduce the data, but with increasing energy the hard component (parton collisions with high transferred momenta) grows in importance. This component is supposed to be the dominant one at LHC energies. The need of including hard parton scattering is demonstrated in Fig. 8. At $E_{\text{c.m.}} = 200$ GeV, the model is not able to describe the transverse momentum distribution in the whole p_t region; agreement exists only for $p_t \leq 1.5$–2 GeV/c.

Up to now, a unified treatment of both soft and hard components of high energy hadronic interactions does not exist. The final states obtained in hard processes can be described in term of strings spanned between the quarks, where gluons are treated as internal kink excitations on strings [30]. Hard perturbative processes lead to kinky string states, while soft processes lead to longitudinal strings. There are different phenomenological approaches, which try to combine soft and hard parton interactions. In the Regge theory language, it means the combination of exchanges of "soft" and "hard" Pomerons. The most popular is the eikonal approach [31–34], in which the probability to have a hard parton interaction (a "hard" cut Pomeron) is obtained from the jet production cross section, by using an eikonal unitarization procedure.

In the simulations presented in this section, we assume that each parton-parton collision can be a hard one with probability $w(s)$, which is a function of the initial hadron energy $\sqrt{s}$. A soft collision is treated in the way described in Sec. II. A hard collision goes through a gluon-gluon ($gg \to gg$) hard scattering, using the PYTHIA program [21] to simulate it. Since the parton cross sections diverge for $p_t \to 0$, a cutoff $p_t^{\min} = 2.3$ GeV/c is introduced. The EHLQ set 1 structure functions [35], inserted in the PYTHIA program as a default parameter, are used in these calculations. In the case of several n hard collisions for gluons belonging to the same hadron, the joint structure function should be used; here, each collision is considered independent, except for $\sum_{i=1}^{n} x_i \sim 1$; the same is true in the case of both soft and hard collisions, using the structure functions of Eq. (8) for the soft partons and the EHLQ structure functions for the hard ones.

Some comparison to experimental data can be seen in Fig. 9. To calculate the distributions shown in this figure, we used $w(s) = 1 - \exp[-0.025(s - 376.4)^{0.03}]$. The gluon radiation associated with the hard scattering (glu-

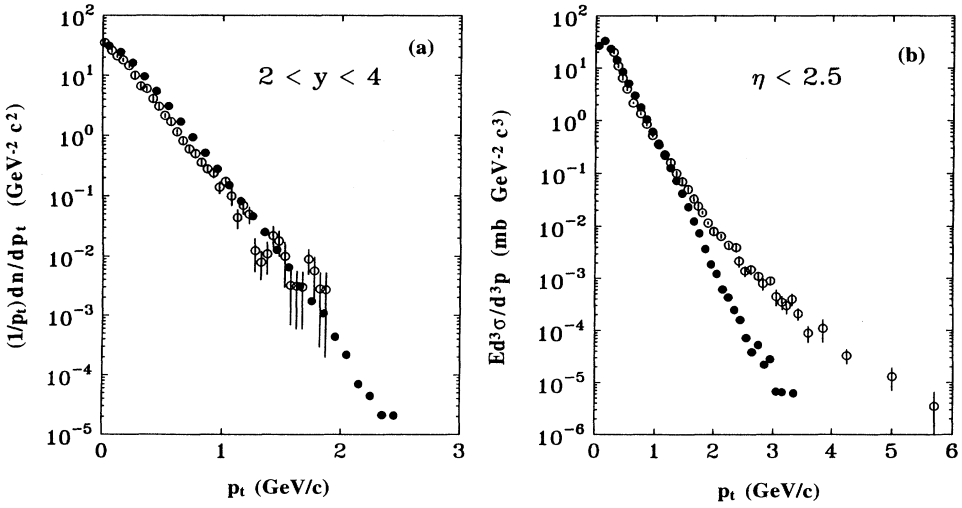

FIG. 8. (a) Transverse momentum distributions of charged particles in the rapidity interval $2 < y < 4$ in pp collisions at $E_{\text{c.m.}} = 19.4$ GeV. (b) Invariant inclusive cross sections of charged particles in the pseudorapidity region $|\eta| \leq 2.5$ in $p\bar{p}$ collisions at $E_{\text{c.m.}} = 200$ GeV. Black points are model predictions; open points are experimental data [29].

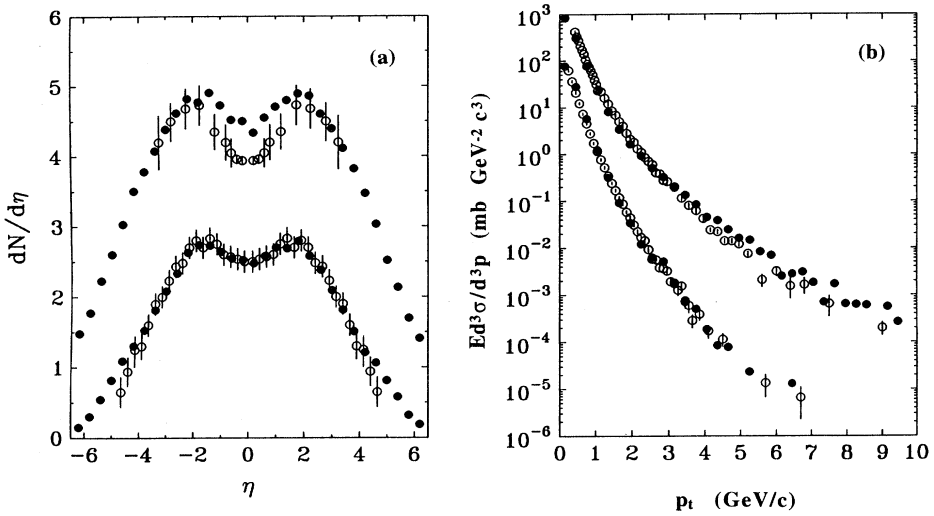

FIG. 9. (a) Pseudorapidity distributions and (b) invariant inclusive cross sections of charged particles in $p\bar{p}$ collisions at (from the bottom to the top) $E_{\rm c.m.} = 200$ and 1800 GeV. Black points are model predictions; open points are data [28,29]. Both the calculations and experimental data [29] in the invariant inclusive cross sections are obtained in the pseudorapidity region $|\eta| \leq 2.5$ and $|\eta| \leq 1$ at $E_{\rm c.m.} = 200$ and 1800 GeV, respectively.

ons or string ends act as sources of dipole radiation) was simulated by the ARIADNE code [36]. The Lund string fragmentation model [21,37] was applied to simulate the decay of the kinky strings. The default parameters of these programs were used during the simulations.

This is the simplest, straightforward extension of our model to include the hard component. With this choice of the probability $w(s)$ and the introduced $p_t^{\rm min}$ the increasing minijet content with rising energy can be reproduced without changing the inelastic cross section. This is so because this cross section is basically controlled by the Pomeron intercept (which is no longer "soft," but an effective one, containing contributions from both the soft and hard components). An increase of $p_t^{\rm min}$ with energy, such as the one proposed in Ref. [38], could be used if we conveniently redefine $w(s)$.

It follows from our calculations that it is possible to predict the shape of the pseudorapidity distributions and the increase of the central pseudorapidity density with energy for both versions of the model: the pure "soft" version, in which neither hard gluon scattering nor gluon radiation are included, and the "hard+soft" version, with both effects included. But only the latter gives reasonable predictions for p_t distributions.

V. MODEL PREDICTIONS FOR HEAVY ION BEAMS

In this section, some predictions for heavy-ion collisions at energies $E_{\rm c.m.} = 19.4A$ GeV and $E_{\rm c.m.} = 200A$ GeV are presented. So far all calculations discussed be-

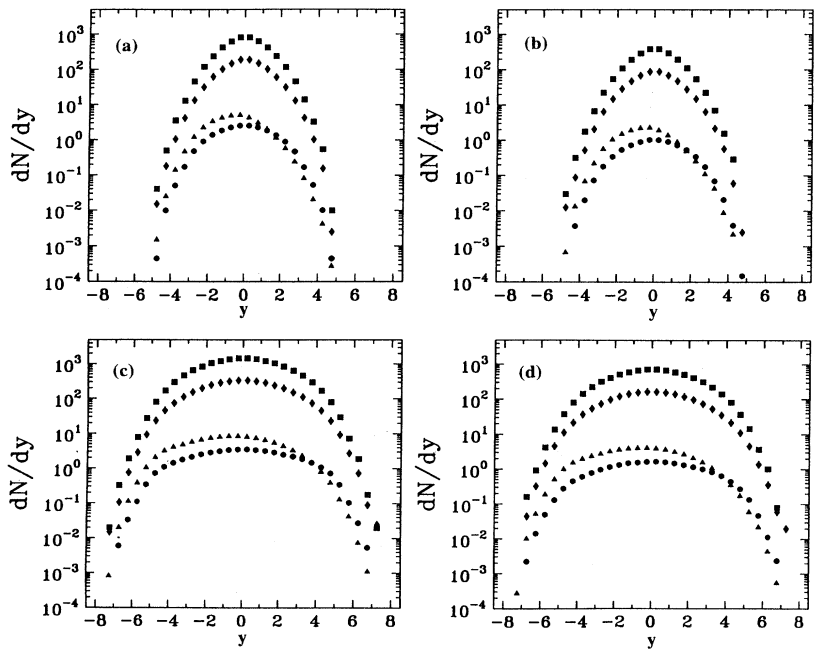

FIG. 10. Model predictions for rapidity distributions of charged [(a),(c)] and negative [(b),(d)] particles produced in (from the bottom to the top) pp, pAu, AuAu, and central AuAu collisions at $E_{\rm c.m.} = 19.4A$ GeV [(a),(b)] and $200A$ GeV [(c),(d)].

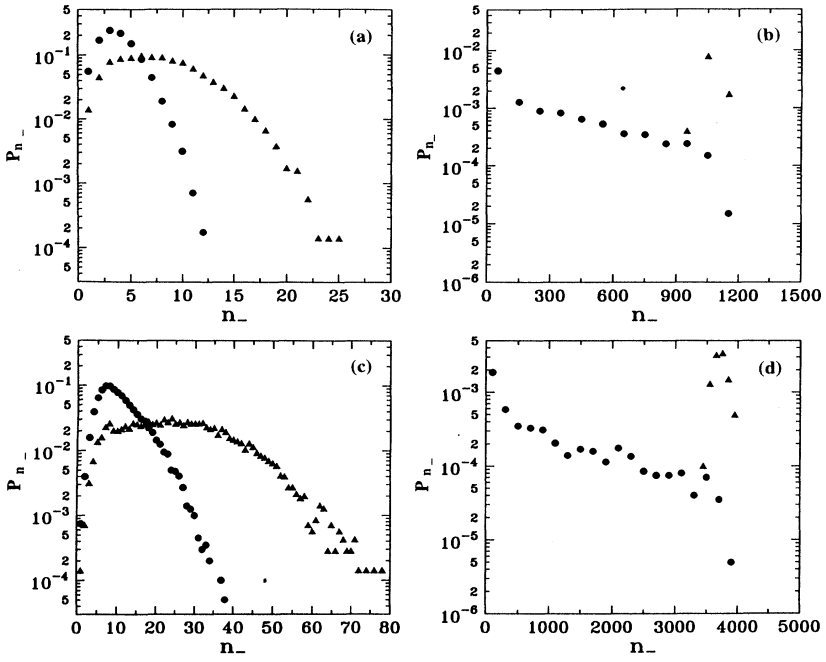

FIG. 11. Model predictions of negative particle multiplicity distributions in the whole rapidity interval in pp (black points) and pAu (triangles) collisions [(a),(c)] and in AuAu (black points) and central AuAu (triangles) collisions [(b),(d)], at $E_{\text{c.m.}} = 19.4A$ GeV [(a),(b)] and $200A$ GeV [(c),(d)].

low have been done without hard gluon scattering and gluon radiation.

A. Light flavor particle production

Charged and negative particle rapidity distributions are shown in Fig. 10 for pp, pAu, AuAu, and central AuAu collisions. The values of the maximum of the charged rapidity density are ~ 800 and ~ 1600 at SPS and RHIC energies, respectively, for central AuAu collisions. This is more or less close to existing calculations [13].

Negative particle multiplicity distributions are presented in Fig. 11 (integrated over the whole rapidity space). The production of about 1000 particles in central AuAu collisions, as well as the narrowness of the multiplicity distribution, point out the possibility to make a one-per-one event experimental analysis.

Some other event characteristics are presented in Tables III(a) and III(b). Our model does not take into account nucleon elastic scattering nor diffraction dissociation nor secondary rescatterings of the produced hadrons in the nuclear medium. Therefore the number of nucleons should be strongly underestimated.

Two factors are essential to produce strange hadrons, baryon-antibaryon pairs, and charmed hadrons: suppression parameters for the string decay, and string masses. String masses depend on the structure functions, on the x cuts, on the initial energy, and on the size of the colliding system. In central AuAu collisions at $E_{\text{c.m.}} = 19.4A$ GeV, the initial energy is shared among about 1000 strings. This leads to a kinematical suppression of heavy hadrons. The influence of this kinematical factor is much less at RHIC energy, as can be seen in Tables III(a) and

TABLE III. (a). Number of events (N_{evt}), particle production cross sections (σ_{prod}), and mean multiplicities of charged particles (n_{ch}), negative particles (n_{neg}), charged pions ($n_{\pi^\pm}$), charged kaons ($n_{K^\pm}$), protons (n_p), neutrons (n_n), antiprotons ($n_{\bar{p}}$), and lambdas (n_Λ), and the difference between the initial nucleon rapidity and the position of the maxima in rapidity net proton distributions ($y_0 - y_{\text{max}}$), in pp, pAu, AuAu, and central AuAu collisions at $E_{\text{c.m.}} = 19.4A$ GeV. (b) The same as (a), at $E_{\text{c.m.}} = 200A$ GeV.

Reaction	pp	pAu (a)	AuAu	AuAu$_c$
N_{evt}	40 000	14 000	2000	200
σ_{prod} (mb)	28.58	1642.7	6573.2	
n_{ch}	8.75	17.35	535.66	2263.3
n_{neg}	3.26	7.84	252.2	1066.4
$n_{\pi^\pm}$	6.67	14.34	454.1	1923.1
$n_{K^\pm}$	0.63	1.16	39.02	168.35
n_p	1.26	1.67	38.50	156.46
n_n	0.69	1.68	45.74	180.02
$n_{\bar{p}}$	0.058	0.084	1.740	6.860
n_Λ	0.157	0.247	5.544	21.64
$y_0 - y_{\text{max}}$	0.92	2.32		1.74
		(b)		
N_{evt}	20 000	7000	1000	100
σ_{prod} (mb)	43.56	1776.8	6810.9	
n_{ch}	19.62	53.11	1719.7	7575.7
n_{neg}	8.83	25.66	843.40	3717.3
$n_{\pi^\pm}$	15.65	44.82	1470.7	6492.5
$n_{K^\pm}$	2.00	4.61	153.83	678.84
n_p	1.54	2.45	58.99	247.25
n_n	0.93	2.62	66.57	271.38
$n_{\bar{p}}$	0.331	0.691	20.99	91.840
n_Λ	0.340	0.714	18.21	74.89
$y_0 - y_{\text{max}}$	1.18	2.78		2.08

III(b). The model fails to reproduce the enhancement of strange baryons in central nucleus-nucleus collisions observed in the NA35 experiment [23]. For this reason, the predictions for strange baryon production in central heavy-ion collisions should be much lower than the experimental data.

It should be stressed that in our model, as in most string models, the produced strings do not interact and decay independently. Introduction of some collective effects, like string fusion [16], can change the predictions essentially, especially for rapidity plateau heights and high multiplicity distribution tails. Also the $\bar{\Lambda}$ enhancement experimentally seen in central SS and SAg collisions at $\sqrt{S_{NN}} = 19.4$ GeV can be described [39].

B. Charmed particle production

As shown in Sec. III B, the model gives reasonable agreement with the existing data on charm production in pp collisions at $E_{\rm c.m.} = 27.4$ GeV. Production of charmed hadrons in ultrarelativistic heavy-ion collisions offers the opportunity to study different aspects of nuclear reactions, such as the thermalization time [40], multicharmed baryon production in the presence of QGP [41], etc. Predictions on charm production on nuclear targets are given in Table IV. At $E_{\rm c.m.} = 200A$ GeV the model predicts ~ 3 charmed particles in each central event, and the central rapidity density of charmed particles can reach ~ 0.7. This large amount of charmed particles can open interesting perspectives for the creation of high energy neutrino beams [42], particularly for the yet unobserved ν_τ.

C. Nuclear stopping power

In Tables III(a) and III(b) predictions for the relative position of the maxima of the net proton rapidity distributions are presented to illustrate the so-called nuclear stopping power. The rapidity shift is determined by how the total nucleon momentum is divided among partons sitting on the ends of the strings, i.e., by the quark and diquark structure functions and by their number. In our case the number of partons increases with the initial energy. But the rapidity shift is weakly dependent on energy for a given parton number, since the structure function is a product of $(1/\sqrt{x})$'s. With a different sea quark structure function, say $1/x$ as in the DPM [10], the rapidity shift decreases with energy, due to the x cut introduced [43]. The rapidity shift is also dependent on the fragmentation function of a diquark to produce a proton. As follows from our calculations, the rapidity shift per soft parton-parton collision is approximately 0.40–0.45 (no secondary parton or hardon rescattering is included in the model).

D. Meson density evolution

To obtain information about the evolution of the colliding system we use the simple idea of Ref. [44]. In the Lund model [20] the time t_i and coordinate z_i of the hadron i, produced in the string decay, are defined by

$$t_i = (1/2\kappa)\left[M_s - 2\sum_{j=1}^{i-1} p_{z_j}\right] + E_i - p_{z_i}, \qquad (10)$$

$$z_i = (1/2\kappa)\left[M_s - 2\sum_{j=1}^{i-1} E_j\right] + p_{z_i} - E_i, \qquad (11)$$

in the string center of mass. Here index $i = 1, 2, \ldots$ orders the string breakup points, M_s is the string mass, $\kappa \sim 1$ GeV/fm is the string tension, and p_{z_i} and E_i are the hadron longitudinal momentum and energy, respectively. Quarks are assumed to be massless. To find the hadron time and coordinate in the observer frame, Lorentz boosts and rotations are performed. If interactions of hadrons after their production through string decay are neglected, the time evolution of particle and energy density can be calculated, since the time, coordinates, and momenta of the produced hadrons are known. The predictions are very limited by the absence of information about longitudinal coordinates and time of the string formation points. They are assumed to be equal to zero. This is not a realistic assumption, because the low momentum initial partons, whose interaction leads to string formation, should be smeared in longitudinal length; however, it gives the possibility to clearly see a finite hadron production time, presented in Fig. 12 for mesons. In our model mesons are produced only after 0.5–1 fm/c. Since the hadron formation time in this Lund definition [20] is proportional to the transverse hadron mass, baryons are produced later than mesons, after ~ 2

TABLE IV. Mean multiplicities of all charmed hadrons ($n_{\rm charm}$), $D/\bar{D}$ mesons ($n_{D/\bar{D}}$), and maximum rapidity densities of all charmed particles and $D/\bar{D}$ mesons, in pp, pAu, AuAu, and central AuAu collisions at $E_{\rm c.m.} = 200A$ GeV. The number of simulated events is shown in Table III(b).

Reaction	pp	pAu	AuAu	AuAu$_c$
$n_{\rm charm}$	0.0116	0.0252	0.69	2.96
$dn_{\rm charm}/dy$	0.0025	0.0049	0.20	0.7
$n_{D/\bar{D}}$	0.0072	0.0167	0.502	2.06
$dn_{D/\bar{D}}/dy$	0.0016	0.0037	0.15	0.50

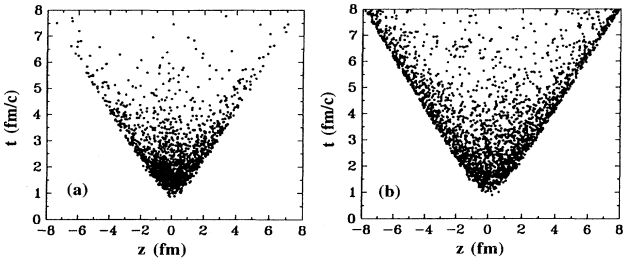

FIG. 12. Space-time picture of meson formation in central AuAu collisions at (a) $E_{\rm c.m.} = 19.4A$ GeV and (b) $200A$ GeV.

fm/c. It is a long time as compared with the temporal evolution extracted from models based on only hard parton scatterings. In particular, at RHIC energy in the hard parton collision model of Ref. [45], after 2 fm/c an equilibrated parton gas can already be established.

To estimate local meson density as a function of time in the center of mass of the colliding nuclei we choose a box with size $L_x = 2$ fm, $L_y = 15.0$ fm, and $L_z = 24$ fm. Space grids are also introduced: $\Delta x = 2$ fm, $\Delta y = 2.5$ fm, $\Delta z = 1$ fm. Evolution of meson particle densities is shown in Fig. 13, starting from 3 fm/c (when the maximum density is approximately reached). At both energies the model predicts approximately equal maxima: $\sim$ 3–3.5 mesons per fm^3, which can be reached after time $t_{\rm c.m.} \sim 3$ fm/c, but at RHIC energy the meson density decreases much more slowly than at SPS energy. After reaching the maxima meson densities fall to ~ 1 meson per fm^3 for ~ 3 fm/c at SPS energy and for ~ 6 fm/c at RHIC energy.

At ultrarelativistic (especially at RHIC) energies, where the produced mesons are concentrated along the light cones, a more suitable evolution parameter is the proper time $\tau = \sqrt{t^2_{\rm c.m.} - z^2_{\rm c.m.}}$, where $t_{\rm c.m.}$ and $z_{\rm c.m.}$ are the center of mass time and longitudinal coordinate of the produced hadron. Using Bjorken's formula [46] for the meson density,

$$\rho_m = (1/\tau A_{\rm trans}) dN/d\eta, \tag{12}$$

where $A_{\rm trans}$ is the Au transverse area, N is the number of mesons produced, and η is the space-time meson rapidity, we can calculate the τ evolution of the meson (and also energy) density of specifying the transverse mass $m_t \approx 0.5$ GeV. The calculated meson density evolution at both energies looks similar. It reaches a sharp maximum: ~ 3.7 mesons per fm^3 at $\tau \sim 2.0$ fm/c and ~ 4 mesons per fm^3 at $\tau \sim 2.5$ fm/c, at SPS and RHIC, respectively. After the maxima, the meson densities decrease quickly, following a longitudinal $(1/\tau)$ expansion.

The existence during 5–7 fm/c of a very dense meson matter is an interesting phenomenon that might deserve intensive studies.

VI. CONCLUSIONS

The Monte Carlo parton string model which is intended for simulation of multiparticle production in NN, NA, and AA collisions at high energies is described.

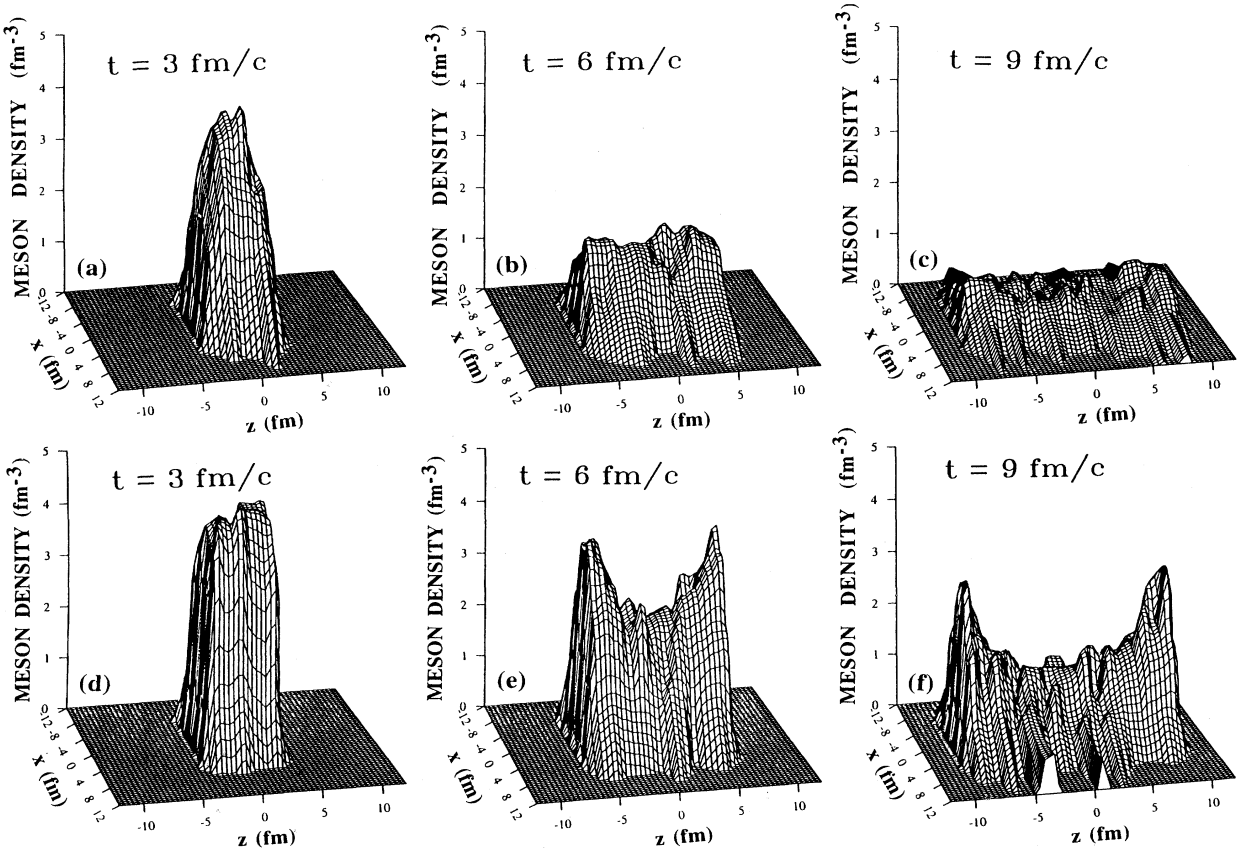

FIG. 13. Meson density evolution in central AuAu collisions. (a), (b), and (c) correspond to $E_{\rm c.m.} = 19.4A$ GeV, and have been calculated at center of mass (of the colliding nuclei) time (a) $t_{\rm c.m.} = 3$ fm/c, (b) $t_{\rm c.m.} = 6$ fm/c, and (c) $t_{\rm c.m.} = 9$ fm/c. (d), (e), and (f) correspond to $E_{\rm c.m.} = 200A$ GeV, and have been calculated at (d) $t_{\rm c.m.} = 3$ fm/c, (e) $t_{\rm c.m.} = 6$ fm/c, and (f) $t_{\rm c.m.} = 9$ fm/c.

Comparison to some available experimental data shows that the model works reasonably well and can be useful to study heavy-ion collisions, as a first approximation.

To make a qualitative analysis we have calculated the mean numbers of both light flavor and charmed hadrons produced in pp, pA, and minimum bias and central AuAu collisions at energies $E_{\text{c.m.}} = 19.4A$ and $200A$ GeV. At both energies and for the mentioned colliding systems rapidity distributions for charged, negative, and charmed hadrons, negative particle multiplicity distributions, net proton rapidity distributions, and meson density evolution have been presented.

We should stress that our simplified model cannot pretend to produce detailed quantitative predictions. First, no hadronic final state rescatterings have been included, which should be important for a more detailed description of nuclear collisions. As we have seen, the meson density can reach ten times the normal nuclear density, so that hadron interactions might be crucial for a correct hadron gas evolution, approaching mechanical and/or chemical equilibrium, and change significantly the hadron momentum distributions or the hadron content. Second, an independent string formation and decay picture has been used as a basis for particle production. With the number of strings growing as energy and atomic number of the colliding particles get larger, one should expect interaction between the strings and their fusion. Some attempts to include this phenomenon have been published in Ref. [16].

An attempt to include hard perturbative parton scattering and gluon radiation has been made. Hard parton scattering is essential to reproduce the transverse momentum distributions for $p_t > 2$ GeV/c, and its effect increases with energy. It also has a time scale different from the one in soft interactions (hard interactions could happen at an earlier stage of the reaction, changing the evolution of the colliding system).

In the literature some studies of multiple particle production at high energies have been published similar to our approach (a DPM Monte Carlo model [32], and an analytical approach [13]). In Ref. [32] predictions are given for the rapidity and transverse momentum distributions and the minijet component of the hadronic energy density for energies up to $E_{\text{c.m.}} = 6300A$ GeV. In Ref. [13] the multiplicities and the spectra of various produced particles (including charm) are studied at $E_{\text{c.m.}} = 200A$ GeV.

These models as well as our model are able to reproduce satisfactorily most of the existing experimental data on nucleus-nucleus collisions. Nevertheless, hadronic densities obtained in present experiments are not so high as to be sensitive to the novel manner of describing the nucleus in terms of partons, employed in our model. We expect that in future experiments, at RHIC or LHC energies, with nuclear densities substantially higher, our approach will be more satisfactory than those quoted above (only valid at low hadronic densities). Another advantage of treating hadronic and nuclear interactions in a similar manner is the easy way in which interaction between the color strings can be introduced (as in Ref. [16]). In addition, charm production is included in the fragmentation scheme, which is not very common in other Monte Carlo fragmentation procedures. As for concrete results, our predictions are consistent with those of Refs. [32,13], except for some specific observables: e.g., we predict 5–7 times more charmed $D/\bar{D}$ mesons in AuAu collisions at RHIC energy than in Ref. [13].

ACKNOWLEDGMENTS

The authors are grateful to the Alexander von Humboldt Foundation and the CICYT of Spain for financial support.

[1] *Quark Matter '90*, Proceedings of the Collision, Meudon, Eighth International Conference on Ultrarelativistic Nucleus-Nucleus Collision, Meudon, France, 1990, edited by J. P. Bleizot, C. Gerschel, B. Pire, and A. Romana [Nucl. Phys. **A525**, 1 (1991)].

[2] B. Andersson, G. Gustafson, and B. Nilsson-Almqvist, Nucl. Phys. **B281**, 289 (1987); B. Andersson, G. Gustafson, and Hong Pi, Z. Phys. C **57**, 485 (1993).

[3] H. Sorge, H. Stöcker, and W. Greiner, Nucl. Phys. **A498**, 567c (1989); H. Sorge, A. von Keitz, R. Matiello, H. Stöcker, and W. Greiner, Phys. Lett. B **243**, 7 (1990); A. von Keitz, H. Sorge, H. Stöcker, and W. Greiner, Nucl. Phys. **A527**, 601 (1991).

[4] K. Werner, Phys. Rep. **232**, 87 (1993).

[5] H.-J. Möhring, A. Capella, J. Ranft, J. Tran Thanh Van, and C. Merino, Nucl. Phys. **A525**, 493c (1991).

[6] N. S. Amelin, K. K. Gudima, and V. D. Toneev, *The Nuclear Equation of State, Part B*, edited by W. Greiner and H. Stöcker, NATO Advanced Study Institute Series Series B: Physics Vol. 216 (Plenum, New York, 1989), p. 473; N. S. Amelin, L. P. Csernai, K. K. Gudima, V. D. Toneev, and S. Yu. Sivoklokov, Phys. Rev. D **47**, 1413 (1993).

[7] L. V. Gribov, E. M. Levin, and M. G. Ryskin, Phys. Rep. **100**, 1 (1983).

[8] K. G. Boreskov and A. B. Kaidalov, Yad. Fiz. **48**, 575 (1988) [Sov. J. Nucl. Phys. **48**, 367 (1988)]; Acta Phys. Pol. **B20**, 397 (1989).

[9] N. Armesto, M. A. Braun, and C. Pajares, Phys. Rev. C **51**, 3393 (1995).

[10] A. Capella, U. P. Sukhatme, C.-I. Tan, and J. Tran Thanh Van, Phys. Rep. **236**, 225 (1994).

[11] A. B. Kaidalov, Nucl. Phys. **A525**, 39c (1991); Sov. J. Nucl. Phys. **45**, 902 (1987); A. B. Kaidalov and O. I. Piskunova, Z. Phys. C **30**, 145 (1985).

[12] G. I. Lykasov and M. N. Sergeenko, Z. Phys. C **56**, 697 (1992).

[13] Yu. M. Shabelskii, Sov. J. Nucl. Phys. **55**, 1399 (1992); Z. Phys. C **57**, 409 (1993).

[14] I. Sarcevic and P. Valerio, Phys. Lett. B **338**, 426 (1994).

[15] Yu. M. Shabelskii, Sov. Sci. Rev. A Phys. **17**, part 2, 1 (1993); L. Cifarelli, E. Eskut, and Yu. M. Shabelskii, Nuovo Cimento A **106**, 389 (1993).

[16] N. S. Amelin, M. A. Braun, and C. Pajares, Phys. Lett. B **306**, 312 (1993); Z. Phys. C **63**, 507 (1994); in *Proceedings of the XXII International Symposium on Multi-*

particle Dynamics, Santiago de Compostela, 1992, edited by C. Pajares (World Scientific, Singapore, 1993), p. 482.
[17] V. A. Abramovskii, E. V. Gedalin, E. G. Gurvich, and O. V. Kancheli, Sov. J. Nucl. Phys. **53**, 271 (1991).
[18] X. Artru and G. Mennessier, Nucl. Phys. **B70**, 93 (1974); X. Artru, Phys. Rep. **97**, 147 (1983).
[19] R. D. Field and R. P. Feynman, Nucl. Phys. **B136**, 1 (1978).
[20] B. Andersson, G. Gustafson, G. Ingelman, and T. Sjöstrand, Phys. Rep. **97**, 31 (1983).
[21] T. Sjöstrand, Comput. Phys. Commun. **39**, 347 (1986); CERN Report No. CERN-TH 6488, 1992; T. Sjöstrand and H.-U. Bengtsson, Comput. Phys. Commun. **43**, 367 (1987).
[22] C. De Marzo *et al.*, Phys. Rev. D **26**, 1019 (1982).
[23] J. Bartke *et al.*, Z. Phys. C **48**, 191 (1990); R. Stock *et al.*, Nucl. Phys. **A525**, 221c (1991).
[24] T. Åkesson *et al.*, CERN Report No. CERN-EP 111, 1989.
[25] M. Aguilar-Benítez *et al.*, Phys. Lett. B **201**, 176 (1988).
[26] R. E. Ansorge *et al.*, Z. Phys. C **41**, 179 (1988).
[27] R. E. Ansorge *et al.*, Z. Phys. C **43**, 357 (1989).
[28] G. J. Alner *et al.*, Z. Phys. C **33**, 1 (1986).
[29] A. Bamberger *et al.*, Z. Phys. C **38**, 89 (1988); C. Albajar *et al.*, Nucl. Phys. **B335**, 261 (1990); F. Abe *et al.*, Phys. Rev. Lett. **61**, 1819 (1988).
[30] B. Andersson, G. Gustafson, and B. Söderberg, Nucl. Phys. **B264**, 29 (1986).
[31] T. Sjöstrand and M. van Zijl, Phys. Rev. D **36**, 2019 (1987).
[32] I. Kawrakov, H.-J. Möhring, and J. Ranft, Phys. Rev. D **47**, 3849 (1993).
[33] X.-N. Wang and M. Gyulassy, Phys. Rev. D **45**, 844 (1992).
[34] N. S. Amelin, E. F. Staubo, and L. P. Csernai, Phys. Rev. D **46**, 4873 (1992).
[35] E. Eichten, I. Hinchliffe, K. Lane, and C. Quigg, Rev. Mod. Phys. **56**, 579 (1984).
[36] B. Andersson, G. Gustafson, L. Lönnblad, and U. Pettersson, Z. Phys. C **43**, 625 (1989); U. Pettersson, Lund Report No. LU TP 88-5, 1988; L. Lönnblad, Lund Report No. LU TP 89-10, 1989.
[37] T. Sjöstrand, Nucl. Phys. **B248**, 469 (1984).
[38] F. W. Bopp, D. Pertermann, R. Engel, and J. Ranft, Phys. Rev. D **49**, 3236 (1994).
[39] N. Armesto, M. A. Braun, E. G. Ferreiro, and C. Pajares, Phys. Lett. B **344**, 301 (1995).
[40] B. Müller and X.-N. Wang, Phys. Rev. Lett. **68**, 2437 (1992).
[41] P. Lèvai and J. Zimànyi, Phys. Lett. B **304**, 203 (1993).
[42] A. De Rújula, E. Fernández, and J. J. Gómez-Cadenas, CERN Report No. CERN-TH 6452, 1992.
[43] J. A. Casado, Phys. Lett. B **309**, 431 (1993).
[44] K. Werner, Phys. Lett. B **219**, 111 (1989).
[45] K. Geiger and B. Müller, Nucl. Phys. **B369**, 600 (1992).
[46] J. D. Bjorken, Phys. Rev. D **27**, 140 (1983).